Advanced Sciences and Technology Journal

ASTJ vol. 3 no.1 (2026) P1048
10.21608/astj.2025.352770.1048
https://astj.journals.ekb.eg/

Deep Learning-Based Synthetic Brain Images from CT/MRI Data: A Review

Ahmed S. El-Hossiny *, Mostafa El-Hussien Ibrahem, Abdel Rahman Shaaban
Biomedical and Systems Engineering Department, Higher Institute of Engineering, El-Shorouk Academy, Cairo, 11837, Egypt
*a.elhossiny@sha.edu.eg

ARTICLEINFO

Article history:
Received 13 January 2025
Revised 13 March 2025
Accepted 22 August 225
Available online 7 October 2025

Handling Editor:
Prof. Dr. Mohamed Talaat Moustafa

Keywords:
Deep learning,
Generative Adversarial Networks,
Paired Data,
Unpaired Data,
Synthetic CT.

ABSTRACT

Generative Artificial Intelligent models have emerged as powerful tools in various specialties, revolutionizing the landscape of image synthesis. In the medical field, Generative Adversarial Networks (GANs) have shown tremendous potential for addressing critical challenges and unlocking new opportunities for programmers. This review provides an overview of the applications of GANs for medical image synthesis for the human brain, through magnetic resonance imaging (MRI) and computed tomography (CT) images discussing their role in generating realistic and diverse medical images for training robust machine learning models. The review paper discusses the need for large, annotated datasets, the differences that can be influenced by the data being paired or unpaired, the quantity of the image data set, the usage of different types of GANs and other deep learning (DL) methods for the brain modality translation, and comparing the results of mean absolute error (MAE), peak signal-to-noise ratio (PSNR), and structural similarity index measure (SSIM) for papers from 2017 to 2023.

1. Introduction

The emergence of synthetic images or image-to-image translation techniques in the medical field as a modern tool has led to competition among programmers, especially in techniques and methods based on artificial intelligence, such as machine learning and deep learning (DL), to create new medical services and applications. Since then, synthetic image methods or generative models have opened numerous avenues for addressing complex medical image analysis issues, including denoising, reconstruction, segmentation, data simulation, detection, and classification. Their capacity to generate highly realistic images raises the possibility of alleviating the persistent shortage of data. Examples of applications include enhancing the image quality of low-dose computed tomography (CT) scans and low-dose positron emission tomography (PET) scans, reconstructing CT images from multi-dimensional X-ray images, facilitating fusion processes for different imaging modalities, generating synthetic 3T magnetic resonance imaging (MRI) from 1.5T images, and producing synthetic CT images from MRI images, or vice versa, for organs and body areas such as the brain, neck, spinal cord, chest, and hip.

Many factors lead to the creation of synthetic images, such as cost reduction, minimization of waiting time, or the need for different imaging devices. To enhance the quality of images, especially when there is noise and artifacts in the images, low radiation doses, or limitations of devices. Needing to avoid using some devices due to their side effects. In addition, synthetic medical images generated to extract more information from images [1], [2].

Programmers compete to design the best generative model for creating synthetic medical images to achieve accurate and realistic output in the minimum possible time. To achieve this, the model must meet the following two criteria at the implementation stages:

1.1. Selection Of the Optimal Dataset:

The primary role of the data is to build the model so that the limits of the model are represented by the data it is trained on, and the more high-quality datasets it trains on, the higher quality and realistic it is given. Data are described with simple details, such as the number of patients, their ages, gender, general health conditions, date, type of imaging, and size of the image. The dataset collection was performed in two ways. The first way is to collect data manually from hospitals and medical diagnostic imaging centers. Second, data can be collected from image datasets on websites such as The Cancer Imaging Archive (TCIA), FreeSurfer

(software suite), and OpenNEURO. Also, some projects have combined these two methods when collecting data to obtain the most information possible. In addition, paired datasets are always preferred over unpaired datasets, as they help in predicting synthetic images based on real data on which the model was based, Figure 1 defines the difference between data types. Increasing the training dataset can be a good choice through augmentation under conditions and limits to avoid fitting model problems.

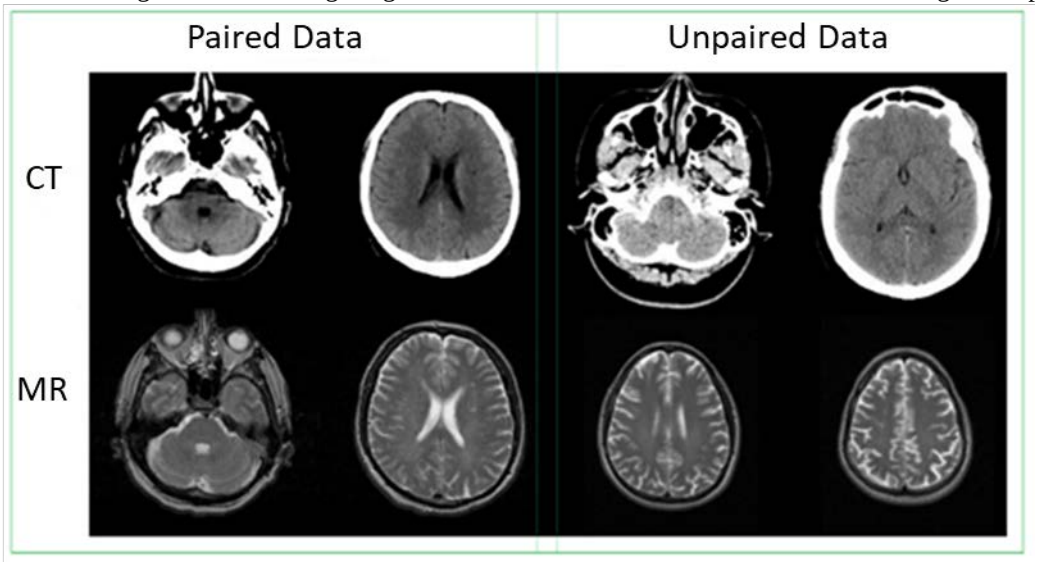

Figure 1. Figure shows the difference between each paired and unpaired dataset for the brain region, images from the Institutional Review Board (IRB) [3].

1.2. Choosing Model Technique:

Choosing a DL model that fits the data well and produces reliable predictions is considered the most important part because it depends on the programmer's skills and the information he possesses. DL model examples, such as generative adversarial network (GAN/GANs) and their models that extend on it, like pixel-to-pixel (pix2pix) (where generator depend on U-Net and discriminator use PatchGAN)[4], conditional or controllable generative adversarial network (cGAN) (which is extends on classing the input labels) [5], deep convolutional generative adversarial network (DCGAN) (extends on CNN architecture), or models that scale up GANs architecture, such as Wasserstein generative adversarial network (WGAN) (discriminator training on data at less time than generator, by enhancing loss function) [6], CycleGAN (a generative model that translates images from source to target) [7],[8],[6]. Anyone who works on GANs has two main components. The first part is called the generator (G) which learns to generate new random data. The second part called the discriminator (D) learns to classify the generator's fake and real data, those processes or game between D and G rebate in this time generator is updating from impact of the loss function, until the discriminator can't be able to distinguish fake data. The target of any generative model is to provide the best measurable results and outcomes closest to realism. Alternatively, a new model is designed based on the previously mentioned methods by changing the nature of both generator and discriminator with an increasing number of the model's layers and functions, enhancing the model's loss function of generator and discriminator.

In this paper, we discuss 30 papers and articles that we reviewed about synthetic CT images based on MRI images and synthetic MRI images based on CT images of the human brain. Our exploration uncovered several compelling reasons that drive the creation of synthetic brain images utilizing CT and MRI. The common reasons for generating synthetic brain images using CT and MRI include the elimination of risks associated with ionizing radiation from CT scans, reduction in both time and financial resources required for multiple different imaging methods, obtaining advantages tailored to each imaging modality, such as imaging soft tissues for MRI and bones for CT scans, and the risks of using each of them for some medical conditions [9]. We discuss these reasons in detail in the medical background, as mentioned in previous papers and articles.

2. Background

From Figure 2, synthetic medical imaging projects with an average of three to four brain applications are created each year, with the creation of synthetic CT images clearly superior to MRI. We also think that the reason for this may be related to the difficulty of conversion to MRI or not taking into consideration the reason for the unavailability of the device in some poor countries and focusing on reducing the radiation risk only. It was also noted that there are few projects on converting CT images to MRI images.

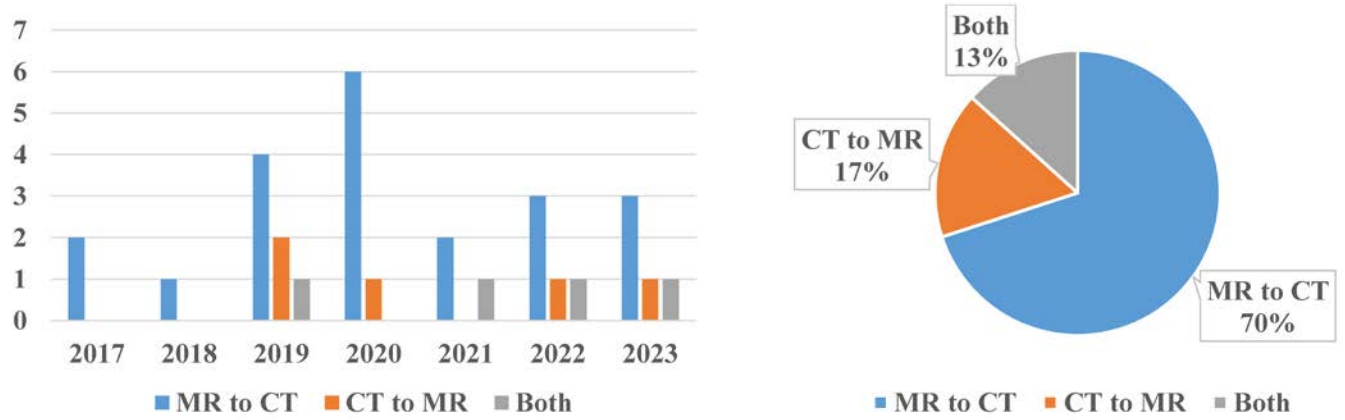

Figure 2. Shows the distribution and percentages of 30 research papers in the field of synthetic medical images for the brain over the past few years. 21 papers from CT to MRI, five papers from MRI to CT, and four papers that apply both modalities. Peak productivity was in 2019 and 2020, when a total of seven papers and articles were published.

2.1. Medical Background

The medical purposes that call for a synthetic CT or MRI procedure are common in most papers. Common reasons for synthetic medical images include eliminating risk, reducing cost, and reducing waiting time. One of the primary reasons for generating synthetic CT images from MRI data is to remove the risk of ionizing radiation [9], CT images are suitable for bony structure [10], and provide electron density information [11], [12]. For MRI synthesis from CT images, CT scans are used as an initial evaluation because of their lower price and faster use; however, MRI is highly contrast and accurate in the diagnosis of diseases such as cancer and stroke [13], [14]. Hospitals in remote rural areas may not have MRI machines [15]. MRI has a higher cost than CT scans in imaging sessions, and individuals with metal implants, strips [3], or pacemakers may be unable to safely use MRI because of its magnetic nature.

2.2. Software Background

The most widely used methods for brain image translation are pix2pix, cGAN, CycleGAN, DCGAN, and U-Net. Spatial papers and articles focused on forming new structures or combining convolutional layers to achieve the best results. Let's take two examples to illustrate this point about the changing on CycleGAN loss function:

$$L_{cycle}(G,F) = Ex_{\sim pdata}(x)\left|\left(G(x)\right) - x\right|_1 + Ey_{\sim pdata}(y)\left|G\left(F(y)\right) - y\right|_1$$

$$L_{DC\text{-}cycle}(G,F,D_X,D_Y) = L_{GAN}(G,D_Y,X,Y) + L_{GAN}(F,D_X,Y,X) + \alpha L_{cycle}(G,F)\ [7]$$

dual contrast CycleGAN (DC-cycleGAN), which is used to synthesize MRI images from CT and vice versa with two generators and two Discriminators like CycleGAN and consist of DC loss. DC-cycleGAN loss function:

$$L_{DC-cycle}(G,F,D_X,DY) = L_{GAN}(G,D_Y,X,Y) + L_{GAN}(F,D_X,Y,X) + \beta L_{DC}(D_Y,X,Y) + \beta L_{DC}(D_X,Y,X) + \alpha L_{scycle}(G,F)$$

$$L_{scycle}(G,F) = SSIM\ (F(G(x)),x) + SSIM(F\left(G(y)\right),y)$$

Where β and α control the equation weight, the method achieves better results than cycleGAN, where the results for MRI synthesis are MAE = 0.04559, PSNR = 26.68858, and SSIM = 0.82622 for the DC-cycleGAN model, and MAE = 0.09155, PSNR = 20.63825, and SSIM = 0.71670 for the ordinary cycleGAN model [16]. Also, DC-cycleGAN achieves higher results than CT synthetic.

sc-cycleGAN, which was developed for unpaired synthetic CT images from MRI, was a model developed with two generators, G_{CT} and G_{MR}, and two discriminators, D_{CT} and D_{MR}. This method aims to provide better results. The CycleGAN loss function for this model is: $L_{cycle}\ (G_{CT},G_{MR}) = |G_{CT}(G_{MR}(I_{CT})) - I_{CT}|_1 + |G_{MR}(G_{CT}(I_{MR})) - I_{MR}|_1$ and sc-cycleGAN loss function:

$$L(G_{CT},G_{MR},D_{CT},D_{MR}) = L_{adv}(G_{CT},D_{CT}) + L_{adv}(G_{MR},D_{MR}) + \lambda_1 L_{cycle}(G_{CT},G_{MR}) + \lambda_2 L_{struct}(G_{CT},G_{MR})$$

Where: $L_{adv}(G_{CT},D_{CT}) = D_{CT}(G_{CT}(I_{MR}))_2 + (1 - D_{CT}(I_{CT}))_2$ and $L_{adv}(G_{MR},D_{MR}) = D_{MR}(G_{MR}(I_{CT}))_1\ (1 - D_{MR}(I_{MR}))_2$ results that sc-cycleGAN achieves compared to cycleGAN MAE = 127.59, PSNR = 24.41, and SSIM = 0.773 to MAE = 143.78, PSNR = 23.73, and SSIM = 0.558 [11].

There are also other examples of improvement models not CycleGAN, like Auto-GAN implemented by an autoencoder network and GAN generator [17], MCMP-GAN with five layers consisting of convolutional levels based on U-Net connect with generator and based on the DCGAN method of producing synthetic images [18], and JP-DAM-GAN (jigsaw puzzle- Discriminating Attenuated model- Generative Adversarial Networks) where that model is based on the pix2pix method to convert between MRI modalities [19].

3. Results and Discussion

Every generative model must evaluate and analyze its performance and efficiency, which can be achieved by visual inspection by radiologists or specialized doctors and can also be achieved mathematically using equations and metrics for synthetic images.

3.1. Mathematical Evaluation Metrics

Evaluation of a synthetic image model performance can be achieved by applying measurement metrics as quantitative indicators of the results. Commonly used equations include mean absolute error (MAE) (1), mean square error (MSE) (2), peak signal-to-noise ratio (PSNR) (3), and structural similarity index measure (SSIM) (4). There are also equations such as dice similarity coefficient (DSC) (5), root mean square error (RMSE) (6), relative global error (ERGAS) (7), universal quality index (UQI) (8), and spatial correlation coefficient (SCC) (9).

$$\mathbf{MAE} = \frac{\mathbf{1}}{\mathbf{N \times M}} \sum_{\mathbf{i=1}}^{\mathbf{N}} \sum_{\mathbf{j=1}}^{\mathbf{M}} \left|\mathbf{I(i,j)} - \check{\mathbf{I}}\mathbf{(i,j)}\right|_{\mathbf{i}} \tag{1}$$

$$\mathbf{MSE} = \frac{\mathbf{1}}{\mathbf{N \times M}} \sum_{\mathbf{i=1}}^{\mathbf{N}} \sum_{\mathbf{i=1}}^{\mathbf{M}} \left(\mathbf{I(i,j)} - \check{\mathbf{I}}\mathbf{(i,j)}\right)_{\mathbf{i}}^{\mathbf{2}} \tag{2}$$

$$\mathbf{RMSE} = \sqrt{\mathbf{MSE}} \tag{3}$$

$$\mathbf{PSNR} = \mathbf{10}\log\left(\frac{\mathbf{MAX^2}}{\mathbf{MSE}}\right) = \mathbf{20}\log\left(\frac{\mathbf{MAX}}{\sqrt{\mathbf{MSE}}}\right) \tag{4}$$

$$\mathbf{SSIM} = \left(\frac{(\mathbf{2}\,\boldsymbol{\mu}_{\mathbf{I}}\,\boldsymbol{\mu}_{\check{\mathbf{I}}} + \mathbf{C_1})(\mathbf{2}\,\boldsymbol{\sigma}_{\mathbf{I}\check{\mathbf{I}}} + \mathbf{C_2})}{(\boldsymbol{\mu}_{\mathbf{I}}^{\mathbf{2}} + \boldsymbol{\mu}_{\check{\mathbf{I}}}^{\mathbf{2}} + \mathbf{C_1})(\boldsymbol{\sigma}_{\mathbf{I}}^{\mathbf{2}} + \boldsymbol{\sigma}_{\check{\mathbf{I}}}^{\mathbf{2}} + \mathbf{C_2})}\right) \tag{5}$$

$$\mathbf{DSC} = \frac{\mathbf{2} \times |\mathbf{A} \cap \mathbf{B}|}{|\mathbf{A}| + |\mathbf{B}|} \tag{6}$$

$$\mathbf{ERGAS} = \mathbf{100}\,\frac{\mathbf{R}_{\text{synthetic CT}}}{\mathbf{R}_{\text{actual CT}}}\sqrt{\frac{\mathbf{1}}{\mathbf{n}}\sum_{\mathbf{i=1}}^{\mathbf{n}}\left(\frac{\mathbf{RMSE^2}}{\boldsymbol{\mu}_{\mathbf{I}}^{\mathbf{2}}}\right)_{\mathbf{i}}} \tag{7}$$

$$\mathbf{UQI} = \frac{\mathbf{4}\boldsymbol{\sigma}_{\mathbf{I}\check{\mathbf{I}}}\,\boldsymbol{\mu}_{\mathbf{I}}\,\boldsymbol{\mu}_{\check{\mathbf{I}}}}{(\boldsymbol{\mu}_{\mathbf{I}}^{\mathbf{2}} + \boldsymbol{\mu}_{\check{\mathbf{I}}}^{\mathbf{2}})(\boldsymbol{\sigma}_{\mathbf{I}}^{\mathbf{2}} + \boldsymbol{\sigma}_{\check{\mathbf{I}}}^{\mathbf{2}})} \tag{8}$$

$$\mathbf{SCC} = \frac{\sum_{\mathbf{i=1}}^{\mathbf{N}} \sum_{\mathbf{i=1}}^{\mathbf{M}} (\mathbf{I(i,j)} - \boldsymbol{\mu}_{\mathbf{I}})\,(\check{\mathbf{I}}\mathbf{(i,j)} - \boldsymbol{\mu}_{\mathbf{I}})}{\sqrt{\sum_{\mathbf{i=1}}^{\mathbf{N}} \sum_{\mathbf{i=1}}^{\mathbf{M}} (\mathbf{I(i,j)} - \boldsymbol{\mu}_{\mathbf{I}})^{\mathbf{2}} \sum_{\mathbf{i=1}}^{\mathbf{N}} \sum_{\mathbf{i=1}}^{\mathbf{M}} \left(\check{\mathbf{I}}\mathbf{(i,j)} - \boldsymbol{\mu}_{\check{\mathbf{I}}}\right)^{\mathbf{2}}}} \tag{9}$$

Error metrics: MAE, MSE, and RMSE. where MAE is used to measure the average distance between the values of synthetic image I and the actual image $\check{\mathbf{I}}$ (1), **i** and **j** refers to the index on the image pixels, N and M refer to dimensions (x, y) of the image, where MSE is similar to MAE but different, the MSE equation calculates the square of average differences, RMSE the root main square for MSE, smaller distance identify smaller error in the results. PSNR (4) is used for evaluating the quality of reconstructed or generated images; MAX refer to the maximum possible pixel value of the image (for example, 255 for 8-bit images($\mathbf{2^n - 1}$)). SSIM or SSI (5) is used for evaluating the quality of images by measuring the structural similarity between a reference image and a synthetic image, where I refers to the synthetic image and $\check{\mathbf{I}}$ refers to an actual image, average or mean (μ), standard division ($\boldsymbol{\sigma}$), $C_1 = (K_1L)^2$ and $C_2 = (K_2L)^2$ where L = MAX value and $K_1 = 0.01$ and $K_2 = 0.02$. By default, the SSIM index ranges from -1 to 1, where 1 indicates perfect similarity between the images, higher SSIM values suggest higher perceived image quality. The DSC (6) is commonly used to measure specific tissue between synthetic and actual images with ranges from 0 to 1. When the

result is close to one, it is close to being the same as the actual image, where A represents the pixels in the predicted mask and B represents the pixels in the ground truth mask. ERGAS (7) was used to measure the quality between synthetic and actual image, where $\left(\mathbf{R}_{\mathbf{synthetic\ CT}}/\mathbf{R}_{\mathbf{actual\ CT}}\right)$ define spatial resolution ratio between the synthesized and actual image. UQI (8) has the same function as the SSIM equation, but it aims to capture both local and global image characteristics, where the output value is between 1 and -1. SCC (9), also known as the spatial correlation index, measures the similarity in spatial patterns between images, and the results range between 1 and -1 [1], [20].

3.2. Discussion And Comparison

From **Table** 1, **Table** 2, and **Table** 3, provide an overview of the modalities of CT and MRI, the methodologies employed, and the corresponding results. The literature surveyed in these tables' spans from 2017 to 2023, with a notable surge in brain-related publications from 2019 as mentioned in the *Figure 2*, indicating a growing interest in and advancements in the field. The keywords used in the search for these papers were GAN, brain CT to MRI, MRI to CT, and synthesis medical images through Google Scholar and the Egyptian Knowledge Bank (EKB). During the search process, we received to number over fifty papers and publications. After careful consideration, we excluded the ones that did not specialize in the brain and head region and Anonymous, as well as those that were published before 2017. In this section, we will provide a comprehensive review and commentary on select papers and articles that we found particularly interesting. In this part of the paper's discussion, the focus will be on the most important observations rather than on all the papers. The previous three comparison tables will be used to summarize everything mentioned earlier in the paper.

TABLE 1
Overview of papers on CT synthesis from MRI (MRI→ CT) for brain images, results focused on MAE, PSNSR, and SSIM, table sorted by publication date.

	Data Quantity	Data Type	DL model	Best Results	Highlights	References & Date
1	270 patients	Paired	3D pix2pix GAN	MAE = 74.28	providing accurate synthetic CT images	Bowen Xin, [12] (2023)
2	50 patients	Paired	Nine CycleGAN models	Model with GAN + L1 and ResNet_3 generator structure is the better with PSNR = 28.76 & SSIM = 0.90	CT synthesis to minimize exposure to cancer radiation therapy	Dr. Teodor Stanescu [20] (2023)
3	95 patients	Unpaired	pix2pix (cGAN)	T1wGd has the best results of MAE = 69.6 ± 12.2 for RC & 71.0 ± 12.2 for LC	give a good identification for the effect of using a different set of MRI images	Lotte Nijskens [21] (2023)
4	26 cancer patients	Paired	WGAN	MAE = 48.39, PSNR = 31.09, & SSIM = 0.9265 dB	Target to eliminate the side effects of radiation	Jiffy Joseph [22] (2022)
5	-----	Unpaired	CycleGAN	-----	This paper focuses on explaining how synthetic image is done	Dalal Rajni Rajnish, [9] (2022)
6	50 patients	Paired	Pix2pix cGAN	PSNR = 29.47	providing a solution for generating synthetic CT images	Chun-Chieh Wang, [23] (2022)
7	41 patients	Paired	U-Net, U-Net++, & Pix2Pix	U-Net++ model is better MAE = 0.082 PSNR = 67.9	U-Net++ Modified method from U-Net	Longfei Zhoua [24] (2021)
8	86 patients	Paired	ResNet, & GAN	ResNet MAE = 114.1±27.5 GAN MAE = 161.3±38.1	Target is to eliminate concerns about using CT	Faeze Gholamiankhah [25] (2021)
9	45 patients	Unpaired	sc-cycleGAN	MAE = 127.59, PSNR = 24.41, & SSIM = 0.773	The paper tried to generate new cycleGAN model and compare it with other Previous attempts	Heran Yang [11] (2020)
10	60 patients	Paired	cGAN	(MAE) = 61 ± 14	development of more effective synthetic for pediatric radiation therapy planning	Matteo Maspero [26] (2020)
11	37 patients	Paired	U-Net	MAE = 60.52 ± 13.32 & PSNR = 49.23 ± 1.92	eliminating the need for CT scanning in the radiotherapy workflow	Bin Tang [27] (2020)
12	32 patients	Paired	MCMP-GAN	MAE = 75.7 ± 14.6, SSIM = 0.92 ± 0.02, & PSNR = 29.1 ± 1.6	generating accurate pseudo-CT images from multi-parametric MRI for nasopharyngeal carcinoma (NPC) patients	Xin Tie [18] (2020)

	Data Quantity	Data Type	DL model	Best Results	Highlights	References & Date
13	45 patients	Unpaired	cGAN	Best results with four channel cGAN MAE = 69.98 ± 12.02, SSIM = 0.85 ± 0.03, & PSNR = 29.39 ± 1.29	Compare between U-Net and cGAN and give a good identification for effect of use a different set of MRI images	Mengke Qi [28] (2020)
14	16 patients	Paired	Auto-GAN	SSIM = 0.9592	Auto-GAN is a multi-modality method	Bing Cao [17] (2020)
15	222 images	Paired	UC-GAN	MAE = 76.7 ± 4.5 & PSNR = 46.1 ± 1.5	Paper compares UC-GAN with cycleGAN	Haitao Wu1 [29] (2019)
16	42 patients	Paired	Pix2pix (cGAN)	MAE_{Body} = 87 ± 11 of 2D sCT Generation	Work on 2D and 3D sCT	Mariana Ferreira [30] (2019)
17	60 patients	Paired	Pix2pix, U-Net, & context-aware	Pix2pix achieved the best results: MAE = 136.9 & PSNR = 46.77	Target to reduce the need for CT scans	Bodo Kaiser [31] (2019)
18	24 patients	Paired	CycleGAN	MAE = 55.7 & PSNR = 26.6	based on dense cycle-consistent generative adversarial networks	Yang Lei [32] (2019)
19	15 patients	Paired	cGAN	Average MAE= 89.30±10.25, SSIM = 0.83±0.03, & PSNR= 26.64±1.17	Target to generating synthetic CT images	Hajar Emami [33] (2018)
20	18 patients	Paired	DCNN	MAE = 84.8 HU	DCNN model near U-net architecture	Xiao Han [34] (2017)
21	24 patients	Paired & Unpaired	CycleGAN	Unpaired: MAE = 73.7 ± 2.3 & PSNR = 32.3 ± 0.7, Paired: MAE = 89.4 ± 6.8 & PSNR = 30.6 ±0.9	Target to synthesize quality CT without using Unpaired data	Jelmer M. Wolterink [35] (2017)

TABLE 2

Overview of papers on MRI synthesis from CT (CT→ MRI) for brain images, results focused on MAE, PSNSR, and SSIM, table sorted by publication date.

	Data Quantity	Data Type	DL model	Best Results	Highlights	References & Date
1	181 patients	Paired	Eight models: UNet V1, V2, Patch, 2D, ++, Attention, Transformer, & CycleGAN	U-Net better results with MAE = 18.29 ± 6.61, PSNR = 21.571 ± 2.724, & SSIM = 0.882 ± 0.030	The paper test U-Net models and compares them with the original structures.	Jake McNaughton [14] (2023)
2	26 patients	Paired	pix2pix	PSNR = 24.30, & SSIM = 0.857	Diagnosing strokes	Na Hu1 [15] (2022)
3	------	------	U-Net with loses functions models, Pix2Pix, & CycleGAN	U-Net, with L1+L2, achieved the best results: MAE = 74.19, PSNR = 32.44, and SSIM = 0.9440	Comparison between methods to find best model	Wen Li [13] (2020)
4	202 patients	Paired & unpaired	MRI-GAN	Paired: MAE =20.34, PSNR =64.28, & SSIM =0.24 Unpaired: MAE =22.94, PSNR =63.77, & SSIM =0.22	MRI-GAN has similar structure to cycleGAN	Cheng-Bin Jin [3] (2019)
5	94 patients	paired	cGAN	-----	Results measured by FCN values.	Jonathan Rubin [36] (2019)

TABLE 3

Overview of both modality (CT↔ MRI) papers of data, model and results measured by MAE, PSNSR, and SSIM equations, table sorted by publication date.

	Data Quantity	Data Type	DL model	Best Results	Highlights	References & Date
1	367 images of CT & MRI	Paired	ADC-cycleGAN	MRI to CT synthesis: MAE = 0.11005, PSNR = 19.04385, SSIM = 0.68551 CT to MRI synthesis: MAE = 0.11080, PSNR = 20.12068, SSIM = 0.65568	Target to high-quality image synthesis	Jiayuan Wang [10] (2023)
2	-----	Unpaired	DC-cycleGAN	MAE = 0.04559, PSNR = 26.68858, & SSIM = 0.82622	contain code resources and comparison with other models	Jiayuan Wang [16] (2022)

	Data Quantity	Data Type	DL model	Best Results	Highlights	References & Date
3	367 paired & 840 unpaired images	Paired & unpaired	uagGAN	Results of paired–unpaired uagGAN models: MRI to CT synthesis: PSNR = 34.786, SSIM = 0.739 CT to MRI synthesis: PSNR = 31.821, SSIM = 0.603	Overcoming the challenges that face the paired and unpaired methods by creating a new paired-unpaired method	Alaa Abu-Srhana [37] (2021)
4	78 patients	Unpaired	DualGAN	CT to MRI synthesis: MAE = 60.83, PSNR = 17.21, & SSIM = 0.8 CT to MRI synthesis: MAE = 37.99, PSNR = 23.31, & SSIM = 0.78	Target to get best result from DualGAN	Denis Prokopenko [38] (2019)

3.2.1. MRI TO CT

From Table 1, we can note that paper No. 4 achieved the best measurable values on all the following: SSIM, PSNR, and MAE. In their study, they used a dataset from the MVR Cancer Center in the DICOM format. Challenges still need to be solved. Paper hinted at it: masking the CT images to filter the noises still has some imperfections due to the CT and MRI differences in data nature. Papers number (No.) 8, 9, and 17 achieved poor numerical results in terms of MAE compared to the rest of the papers. Paper 8 explained that the reason for these limitations was that they worked on one type of data and that the performance of their project could be measured by comparing it with methods such as U-Net. For paper No. 9, their focus was on creating a research paper that would overcome CycleGAN and provide visual inspections. That was mentioned in detail in the "SOFTWARE BACKGROUND" paragraph. They succeeded in their development compared to the ordinary CycleGAN model, but they were not able to achieve high MAE values because of the nature and quality of the training data used. Paper No. 17 achieved reliable results compared with the rest of the models, and they explained their limitations because of the lack of data used. Not all measurements are decisive for deciding about the quality of the model, and visual inspection is a major part of the decision. Why? Because the model's ability to notice small-sized problems, such as tumors and clots, elevates it to the point of reliability, Paper No. 21 represents the effect of using paired and unpaired data mathematically with the CycleGAN model, where the unpaired data achieves better results with the mode due to its nature of dealing with unpaired data. Paper No. 13 helped us to obtain a good idea about the effects of MRI image sequences (T1, T2, T1C, and T1DixonC-water) by applying the cGAN with a 4-channels model to obtain results, which showed that T1 is the best, followed by T1C, T2, and T1DixonC-water they achieve disparity results.

3.2.2. CT TO MRI

Noted that from Table 2 and Table 3 for synthesis MRI images, synthetic MRI does not achieve high-quality image measurements (PSNR, SSIM). The only paper that achieves high image quality was Paper No. 1 and 3 from Table 2, where this paper compares many models to show that the best model, model U-Net (ordinary U-Net), achieved good results over other modifications. U-Net models and ordinary CycleGAN, and the models U-Net_L1+L2 and paired-cycleGAN from paper No. 3 achieved higher results and good visual inspection. From the previous comparisons, it can be concluded that the U-Net models and their improvements achieved the best results in terms of quality and error rate compared to other models. The main reason for the few papers dealing with the synthesis of MRI images from CT is that MRI images contain many details that CT images may fail to capture, which subsequently leads to deficiencies in the synthesis of images. This sensitivity, especially in critical medical decisions like detecting tumors and strokes in brain regions, necessitates heightened efforts and benefits from early diagnostic capabilities.

Across all tables, it is noted that the amount of patient data used increases over time, publishing data for researchers, especially after the coronavirus disease (COVID-19), and we cannot ignore the effect of data on the results, as in some papers, the models achieved results, and the same models achieved lower or higher results in other papers related to the dataset used in building the generative model.

3.3. Summary

The main points noted from papers and articles from the last tables can be summarized as follows. A model's results do not refer to the method's performance; they express the overall model and the data on which it was trained. You cannot show the method's performance until you compare it with other methods with the same input data. Emphasizing the importance of visual inspection for output images from the model. Using unpaired data with the CycleGAN model achieves higher results than paired data. Increasing the volume of data has a positive effect on the model's strong predictive ability, with unpaired data achieving better results. MRI T1 data has shown remarkable superiority and usage in MRI-to-CT translation. U-Net and its variations or GANs model upgrades like Pix2Pix generator, outperform other models in terms of quality and error rate in CT-to-MRI translation.

4. Conclusion

There are still challenges to synthetic medical images spatially with brain synthesis, for example, differences in data nature and complexity between CT and MRI images, which create limitations on MRI synthesis from CT images. Also, a limitation in accessibility to high-quality and paired data. Solving these problems well led to achieving higher results and reliability in this type of project. The review paper also provides a comprehensive overview of the advancements in creating synthetic MRI-CT images for the brain using generative models. The paper discusses the applications of synthetic CT based on MRI and synthetic MRI based on CT for the human brain, highlighting the potential benefits such as cost-effectiveness, and improved imaging quality. We also emphasize the importance of selecting the optimal dataset and choosing the most suitable DL model for generating reliable predictions. The review paper focused on the challenges and limitations in this field, such as the scarcity of projects for converting CT images to MRI images and the difficulty of conversion to MRI. The review also mentioned the computational aspect of models and their types. Overall, the review paper provides valuable insights into the current state and prospects of synthetic MRI-CT imaging for brain applications, offering a foundation for further research and development in this area.

References

[1] X. Yi, E. Walia, and P. Babyn, "Generative adversarial network in medical imaging: A review," *Med. Image Anal.*, vol. 58, Sep. 2019, doi: 10.1016/j.media.2019.101552.

[2] F. Shamshad *et al.*, "Transformers in medical imaging: A survey," *Medical Image Analysis*, vol. 88. Jan. 2023, doi: 10.1016/j.media.2023.102802.

[3] C. Bin Jin *et al.*, "Deep CT to MR synthesis using paired and unpaired data," *Sensors (Switzerland)*, vol. 19, no. 10, pp. 1–19, 2019, doi: 10.3390/s19102361.

[4] P. Isola, J.-Y. Zhu, T. Zhou, and A. A. Efros, "Image-to-Image Translation with Conditional Adversarial Networks," Nov. 2016.

[5] S. O. Mehdi Mirza, "Conditional Generative Adversarial Nets," pp. 1–7, 2014.

[6] A. Thakur and M. Satish, "Generative Adversarial Networks."

[7] J. Zhu, T. Park, A. A. Efros, B. Ai, and U. C. Berkeley, "Unpaired Image-to-Image Translation using Cycle-Consistent Adversarial Networks."

[8] Mohammed Alhami, "Generative Adversarial Networks GANs: A Beginner's Guide," *https://towardsdatascience.com/generative-adversarial-networks-gans-a-beginners-guide-f37c9f3b7817*, Jul. 2020. .

[9] T. Suryawanshi, "Medical image synthesis using GAN," no. July, 2022.

[10] J. Wang, Q. M. J. Wu, and F. Pourpanah, "An Attentive-based Generative Model for Medical Image Synthesis," 2023, doi: 10.1007/s13042-023-01871-0.

[11] H. Yang *et al.*, "Unsupervised MR-to-CT Synthesis Using Structure-Constrained CycleGAN," *IEEE Trans. Med. Imaging*, vol. 39, no. 12, pp. 4249–4261, 2020, doi: 10.1109/TMI.2020.3015379.

[12] B. Xin, A. Nicolson, H. Chourak, and G. Belous, "Team KoalAI : Locally-enhanced 3D Pix2Pix GAN for Synthetic CT Generation," pp. 1–6, 2023.

[13] W. Li *et al.*, "Magnetic resonance image (MRI) synthesis from brain computed tomography (CT) images based on deep learning methods for magnetic resonance (MR)-guided radiotherapy," *Quant. Imaging Med. Surg.*, vol. 10, no. 6, pp. 1223–1236, 2020, doi: 10.21037/QIMS-19-885.

[14] J. McNaughton, S. Holdsworth, B. Chong, J. Fernandez, V. Shim, and A. Wang, "Synthetic MRI Generation from CT Scans for Stroke Patients," *BioMedInformatics*, vol. 3, no. 3, pp. 791–816, 2023, doi: 10.3390/biomedinformatics3030050.

[15] N. Hu *et al.*, "Detecting brain lesions in suspected acute ischemic stroke with CT-based synthetic MRI using generative adversarial networks," *Ann. Transl. Med.*, vol. 10, no. 2, pp. 35–35, 2022, doi: 10.21037/atm-21-4056.

[16] J. Wang, Q. M. J. Wu, and F. Pourpanah, "DC-cycleGAN: Bidirectional CT-to-MR synthesis from unpaired data," *Comput. Med. Imaging Graph.*, vol. 108, no. November 2022, 2023, doi: 10.1016/j.compmedimag.2023.102249.

[17] B. Cao, H. Zhang, N. Wang, X. Gao, and D. Shen, "Auto-GAN: Self-supervised collaborative learning for medical image synthesis," *AAAI 2020 - 34th AAAI Conf. Artif. Intell.*, pp. 10486–10493, 2020, doi: 10.1609/aaai.v34i07.6619.

[18] X. Tie, S. Lam, Y. Zhang, K. Lee, K. Au, and J. Cai, "Pseudo-CT generation from multi-parametric MRI using a novel multi-channel multi-path conditional generative adversarial network for nasopharyngeal carcinoma patients," *Med. Phys.*, vol. 47, no. 4, pp. 1750–1762, Apr. 2020, doi: 10.1002/mp.14062.

[19] X. Z. Can Chang, Li Yao, "A Weakly GAN Combining Global Attention Network in Incomplete Multimodal MRI Synthesis," *SSRN*, p. 14, 2023, doi: 10.2139/ssrn.4463368.

[20] T. Kutlu, "The Investigation of Generative Adversarial Networks for the Generation of Synthetic Computer Tomography Data from Magnetic Resonance Imaging Images for Applications in Adaptive Radiation Therapy for the Central Nervous System," vol. 4, pp. 88–100, 2023.

[21] L. Nijskens, C. A. T. van den Berg, J. J. C. Verhoeff, and M. Maspero, "Exploring contrast generalisation in deep learning-based brain MRI-to-CT synthesis," *Phys. Medica*, vol. 112, no. March, 2023, doi: 10.1016/j.ejmp.2023.102642.

[22] J. Joseph, C. Hemanth, P. Pulinthanathu Narayanan, J. Pottekkattuvalappil Balakrishnan, and N. Puzhakkal, "Computed tomography image generation from magnetic resonance imaging using Wasserstein metric for MR-only radiation therapy," *Int. J. Imaging Syst. Technol.*, vol. 32, no. 6, pp. 2080–2093, 2022, doi: 10.1002/ima.22777.

[23] C. C. Wang *et al.*, "Magnetic Resonance-Based Synthetic Computed Tomography Using Generative Adversarial Networks for Intracranial Tumor Radiotherapy Treatment Planning," *J. Pers. Med.*, vol. 12, no. 3, pp. 1–17, 2022, doi: 10.3390/jpm12030361.

[24] L. Zhou *et al.*, "Synthesizing Human Brain Computed Tomography Images from Magnetic Resonance Images Based on Machine Learning," *SSRN Electron. J.*, 2022, doi: 10.2139/ssrn.3989550.

[25] F. Gholamiankhah, S. Mostafapour, and H. Arabi, "Deep learning-based synthetic CT generation from MR images: comparison of generative adversarial and residual neural networks," *Int. J. Radiat. Res.*, vol. 20, no. 1, pp. 121–130, 2022, doi: 10.52547/ijrr.20.1.19.

[26] M. Maspero *et al.*, "Deep learning-based synthetic CT generation for paediatric brain MR-only photon and proton radiotherapy," *Radiother. Oncol.*, vol. 153, pp. 197–204, 2020, doi: 10.1016/j.radonc.2020.09.029.

[27] B. Tang *et al.*, "Dosimetric evaluation of synthetic CT image generated using a neural network for MR-only brain radiotherapy," *J. Appl. Clin. Med. Phys.*, vol. 22, no. 3, pp. 55–62, 2021, doi: 10.1002/acm2.13176.

[28] M. Qi *et al.*, "Multi-sequence MR image-based synthetic CT generation using a generative adversarial network for head and neck MRI-only radiotherapy," *Med. Phys.*, vol. 47, no. 4, pp. 1880–1894, 2020, doi: 10.1002/mp.14075.

[29] H. Wu, X. Jiang, and F. Jia, *UC-GAN for MR to CT image synthesis*, vol. 11850 LNCS, no. 1. Springer International Publishing, 2019.

[30] M. Ferreira, "A generative adversarial network approach to synthetic-CT creation for MRI-based radiation therapy," *Dissertation*, 2019.

[31] B. Kaiser and S. Albarqouni, "MRI to CT Translation with GANs," 2019.

[32] Y. Lei *et al.*, "MRI-only based synthetic CT generation using dense cycle consistent generative adversarial networks," *Med. Phys.*, vol. 46, no. 8, pp. 3565–3581, Aug. 2019, doi: 10.1002/mp.13617.

[33] H. Emami, M. Dong, S. P. Nejad-Davarani, and C. K. Glide-Hurst, "Generating synthetic CTs from magnetic resonance images using generative adversarial networks," *Med. Phys.*, vol. 45, no. 8, pp. 3627–3636, 2018, doi: 10.1002/mp.13047.

[34] X. Han, "MR-based synthetic CT generation using a deep convolutional neural network method," *Med. Phys.*, vol. 44, no. 4, pp. 1408–1419, Apr. 2017, doi: 10.1002/mp.12155.

[35] J. Wolterink, A. M. Dinkla, M. Savenije, and P. R. Seevinck, "Deep MR to CT Synthesis using Unpaired Data," no. November, 2017.

[36] J. Rubin and S. M. Abulnaga, "CT-To-MR conditional generative adversarial networks for ischemic stroke lesion segmentation," *2019 IEEE International Conference on Healthcare Informatics, ICHI 2019*. pp. 1–11, 2019, doi: 10.1109/ICHI.2019.8904574.

[37] A. Abu-Srhan, I. Almallahi, M. A. M. Abushariah, W. Mahafza, and O. S. Al-Kadi, "Paired-unpaired Unsupervised Attention Guided GAN with transfer learning for bidirectional brain MR-CT synthesis," *Comput. Biol. Med.*, vol. 136, no. August, 2021, doi: 10.1016/j.compbiomed.2021.104763.

[38] D. Prokopenko, J. V. Stadelmann, H. Schulz, S. Renisch, and D. V Dylov, "Unpaired synthetic image generation in radiology using GANs," in *Lecture Notes in Computer Science (including subseries Lecture Notes in Artificial Intelligence and Lecture Notes in Bioinformatics)*, 2019, vol. 11850 LNCS, pp. 94–101, doi: 10.1007/978-3-030-32486-5_12.